First Results from the PHOBOS Experiment at RHIC

Gunther Roland for the PHOBOS Collaboration
B.B.Back[1], M.D.Baker[2], D.S.Barton[2], R.R.Betts[1,6], R.Bindel[7], A.Budzanowski[3], W.Busza[4], A.Carroll[2], M.P.Decowski[4], E.Garcia[7], N.George[1], K.Gulbrandsen[4], S.Gushue[2], C.Halliwell[6], J.Hamblen[8], G.A.Heintzelman[2], C.Henderson[4], R.Hołyński[3], D.J.Hofman[6], B.Holzman[6], E.Johnson[8], J.L.Kane[4], J.Katzy[4], N. Khan[8], W.Kucewicz[6], P.Kulinich[4], W.T.Lin[5], S.Manly[8], D.McLeod[6], J.Michałowski[3], A.C.Mignerey[7], J.Mülmenstädt[4],R.Nouicer[6], A.Olszewski[2,3], R.Pak[2], I.C.Park[8], H.Pernegger[4], C.Reed[4], L.P.Remsberg[2], M.Reuter[6], C.Roland[4], G.Roland[4], L.Rosenberg[4], P.Sarin[4], P.Sawicki[3], W.Skulski[8], S.G.Steadman[4], G.S.F.Stephans[4], P.Steinberg[2], M.Stodulski[3], A.Sukhanov[2], J.-L.Tang[5], R.Teng[8], A.Trzupek[3], C.Vale[4], G.J.van Nieuwenhuizen[4], R.Verdier[4], B.Wadsworth[4], F.L.H.Wolfs[8], B.Wosiek[3], K.Woźniak[3], A.H.Wuosmaa[1], B.Wysłouch[4]

[1] Physics Division, Argonne National Laboratory, Argonne, IL 60439-4843
[2] Chemistry and C-A Departments, Brookhaven National Laboratory, Upton, NY 11973-5000
[3] Institute of Nuclear Physics, Kraków, Poland
[4] Laboratory for Nuclear Science, Massachusetts Institute of Technology, Cambridge, MA 02139-4307
[5] Department of Physics, National Central University, Chung-Li, Taiwan
[6] Department of Physics, University of Illinois at Chicago, Chicago, IL 60607-7059
[7] Department of Chemistry, University of Maryland, College Park, MD 20742
[8] Department of Physics and Astronomy, University of Rochester, Rochester, NY 14627

During the first run of RHIC, the PHOBOS experiment recorded Au+Au collisions at $\sqrt{s_{NN}}$ of 56 GeV and 130 GeV. These data have allowed us to study the energy and centrality dependence of particle production, the anisotropy of the final state azimuthal distribution and particle ratios at mid-rapidity. Our results show a non-trivial evolution of particle densities with both centrality and collision energy, reaching significantly higher values per participating nucleon than at lower energies or in nucleon-nucleon collisions. At $\sqrt{s_{NN}} = 130$ GeV we observe 4100±100(stat.)±400(syst.) charged particles with $|\eta| < 5.4$ for the 3% most central collisions. The observed strong event anisotropy of $v_2^{max} > 0.06$, beyond the value predicted in hadronic cascade models, indicates a closer approach to local thermal equilibration than at lower collision energies. The data on particle ratios show that at $\sqrt{s_{NN}} = 130$ GeV a significant fraction of the incoming baryon number is still shifted towards mid-rapidity. Nevertheless, the resulting baryochemical potential μ_B of about 50 MeV is a factor of 5 lower than at SPS energies.

1. Introduction

In this paper we present data taken with the PHOBOS detector during the first run of the Relativistic Heavy-Ion Collider (RHIC) at Brookhaven Nation Laboratory (BNL). We recorded collisions of Au-nuclei at energies of $\sqrt{s_{NN}} = 56$ and 130 GeV. Ultimately, the goal of our work is to understand the behavior of strongly interacting matter at conditions of extreme density and temperature. Quantum chromodynamics (QCD), the fundamental theory of strong interactions, predicts that for sufficiently high energy density a new state of matter will be formed, the quark-gluon plasma (QGP) [1].

In the first round of data taking at RHIC, the aim of the PHOBOS experiment was to characterize the global conditions achieved in this new energy regime of nuclear collisions. In particular, we tried to obtain information on the overall density of particles produced in the collision, the azimuthal anisotropy of the final state particle distribution and on particle ratios near mid-rapidity. As we will discuss later, these measurements are related to questions of entropy density, the approach to thermal equilibration and the hadro-chemical composition of the particle source.

These data, in particular when interpreted in the context of similar measurements performed at lower collision energies at the CERN SPS and the BNL AGS, provide strong constraints on collision models and should therefore allow more refined predictions for the next round of higher statistics measurements that will be performed in the upcoming run periods. This will include systematic studies of our observables as a function of beam energy and ion species.

2. Experimental setup and event selection

The PHOBOS detector employs silicon pad detectors to perform tracking, vertex detection and multiplicity measurements. An overview of the apparatus is shown in Fig. 1. The main components are the single layer multiplicity detector which covers the pseudorapidity range $|\eta| < 5.4$ with nearly complete azimuthal coverage, a two-layer vertex detector (VTX) covering $|\eta| < 1.5$ and a magnetic spectrometer providing momentum and particle ID information for particles near mid-rapidity (SPECP and SPECN). Details of the experimental arrangement are described in [2,3]. In the initial part of the run, including all of the data taken at $\sqrt{s_{NN}} = 56$ GeV, only a small fraction of the full setup was installed. It included the first 6 layers of the silicon spectrometer (SPEC), part of the two-layer silicon vertex detector (VTX) and one ladder of the large acceptance multiplicity detector. Most of the results shown were obtained using the full setup as shown in Fig. 1, used for data taking at $\sqrt{s_{NN}} = 130$ GeV. In this configuration, the detector had close to 100000 readout channels.

A crucial part of the setup were two sets of 16 scintillator counters ("paddle counters", PP and PN) that detected charged particles in the pseudorapidity range $3 < |\eta| < 4.5$. They served as the primary event trigger and were also used for event selection and determination of the collision centrality. Not shown in Fig. 1 are two zero-degree calorimeters (ZDCP,ZDCN) at $z = \pm 18.5$ m, which provided additional information for event selection by measuring the energy deposited by spectator neutrons.

The online trigger selected events based on the coincidence of at least one hit in both PP and PN within a time window of 38 ns. This trigger was sensitive to 97% of the

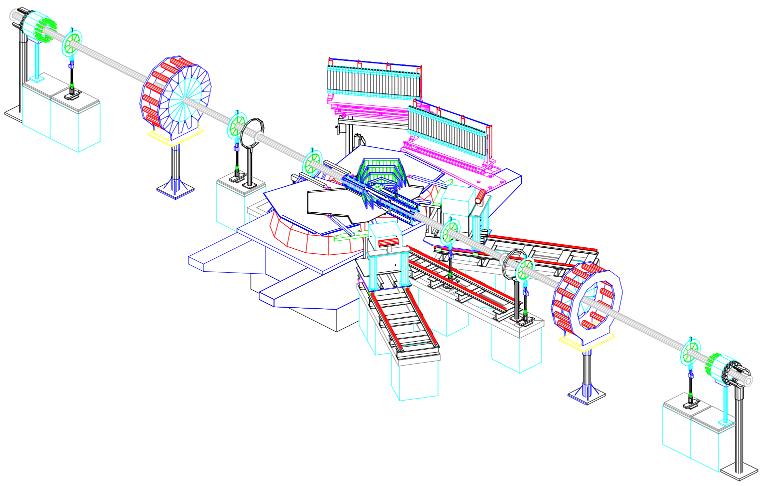

Figure 1. PHOBOS detector setup for the 2000 running period.

inelastic hadronic cross-section. By applying further timing cuts offline, on both the paddle counter and ZDC signals, we achieved an overall background rate of less than 1% of all events. Central events, which were characterized by large signals in both paddle counters, were essentially background-free.

To divide our data set into classes of events according to the number of participating nucleons, we used information from the paddle counters and the zero degree calorimeters. Every event was characterized by a centrality estimator based on the truncated mean of gain-normalized ADC values in the 16 scintillator counters in PP and PN. We estimated the number of participants for the event classes using a Glauber calculation based on HIJING [4] and our GEANT simulation. Details of this procedure can be found in [5].

3. Results

3.1. Energy dependence of $dN_{ch}/d\eta|_{|\eta|<1}$

Charged particle production, as characterized by $dN_{ch}/d\eta$, reflects the time integral of many processes in the evolution of a heavy-ion collision, starting from the initial conditions, e.g. gluon shadowing, the interplay of hard and soft processes in the initial particle production to the effects of re-scattering close to the freeze-out stages. Clearly, a systematic study as a function of system size, collision energy and over a large range of η is needed to disentangle the various effects in comparison to collision models.

The first observable studied was the energy dependence of the charged particle pseudorapidity density near mid-rapidity for central collisions, $dN_{ch}/d\eta|_{|\eta|<1}$. The measurement is described in detail in [6]. It was based on counting two hit-combinations, called tracklets, in consecutive layers of our silicon detectors, with the constraint that the two hits form a straight line pointing to the known primary collision vertex. The result was corrected for backgrounds from decay feed-down, secondary interactions, stopping particles in the beampipe and detector inefficiencies based on the MC simulation of our apparatus.

The data obtained with the initially installed subset of our setup show a primary charged particle density of $dN_{ch}/d\eta|_{|\eta|<1} = 408 \pm 12(\text{stat}) \pm 30(\text{syst})$ for $\sqrt{s} = 56$ AGeV and $555 \pm 12(\text{stat}) \pm 35(\text{syst})$ at $\sqrt{s} = 130$ AGeV. Normalizing per participant pair, we deduce

$dN_{ch}/d\eta|_{|\eta|<1}/(0.5 \times N_{part}) = 2.47 \pm 0.1(\text{stat}) \pm 0.25(\text{syst})$ and $3.24 \pm 0.1(\text{stat}) \pm 0.25(\text{syst})$, respectively.

In Fig. 2 we show the normalized yield per participant obtained for Au+Au collisions, proton-antiproton ($p\overline{p}$) collisions [7] and central Pb+Pb collisions at the CERN SPS [8]. We see that central Au+Au collisions show a significantly larger charged particle density per participant than non-single diffractive (NSD) $p\overline{p}$ collisions at comparable energies. The observed increase of 31% from 56 to 130 AGeV in central Au+Au collisions is significantly larger than the increase shown by a parametrization of $p\overline{p}$ data for the same energy interval [7]. Comparing our data to those obtained at the CERN SPS for Pb+Pb collisions at $\sqrt{s} = 17.2$ AGeV, we find a 70% higher particle density per participant near $\eta = 0$ at $\sqrt{s} = 130$ AGeV. General arguments (c.f. Bjorken's estimate [9]) suggest that this increase should correspond to a similar or larger increase in the maximal energy density achieved in the collision, as the thermalization timescale is expected to be shorter at the higher energy.

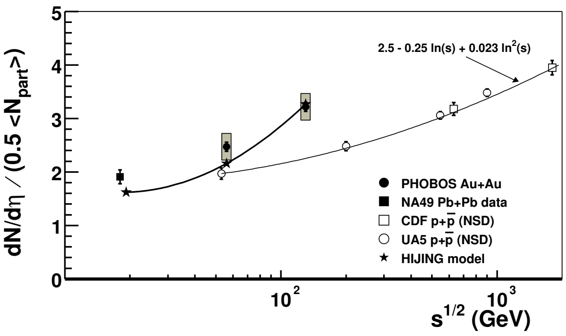

Figure 2. Measured pseudorapidity density normalized per participant pair for central Au+Au collisions. Systematic errors are shown as shaded areas.

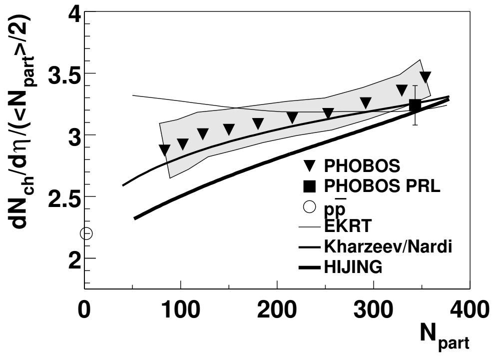

Figure 3. Pseudorapidity density as a function of the number of participants. OFFICIAL STATEMENT ON SYST. ERROR GOES HERE.

3.2. Centrality dependence of $dN_{ch}/d\eta|_{|\eta|<1}$

Model calculations suggest that important additional information on the mechanism responsible for the enhanced particle production observed in central Au+Au collisions can be obtained by studying the particle density as a function of system size [10]. In particular, particle production in soft processes is expected to scale with the volume of the system, whereas hard processes should scale with the number of nucleon-nucleon collisions. This implies a different system size dependence for these two types of processes. Ideally this should be disentangled by studying central collisions of different size ion species. Such a study will hopefully be performed in future running periods at RHIC.

With the present data set, a variation of system size can be achieved by studying $dN_{ch}/d\eta$ for events selected in different bins of fractional cross-section based on the paddle mean, corresponding to a variation in the average number of participants.

The measurement was performed using the full Year-1 configuration of PHOBOS, as shown in Fig. 1. Again, the number of charged particles was obtained by counting the number of tracklets, using data from VTX and the two SPEC subdetectors corrected for various backgrounds. Details of the procedure can be found in [5].

The resulting centrality dependence of $dN_{ch}/d\eta|_{|\eta|<1}$ is shown in Fig. 3. The measurement for central events is in good agreement with the result obtained for a different data set using the initial PHOBOS configuration. As already implied by the comparison to the parametrization of $p\overline{p}$ data for the central data point, the observed centrality dependence does not follow a simple scaling with the number of participants. Rather we observe a steep initial rise from the expected $p\overline{p}$ value to our first data point at $\langle N_{part}\rangle = 83$ and then a slow increase up to our most central bin with $\langle N_{part}\rangle = 353$.

This is qualitatively different from the prediction of HIJING [10], which shows a constant slope in the evolution from $p\overline{p}$ to the most central Au+Au collisions and from the expectations of the EKRT [11] initial state saturation model.

Interestingly, a similar general shape is observed in a measurement of the mid-rapidity charged particle density at lower energies by the WA98 experiment at CERN [12]. They also observe a fast initial increase of $dN_{ch}/d\eta|_{|\eta|<1}/(0.5 \times N_{part})$, followed by a slower increase beyond $N_{part} \approx 100$. In their case, the data are well described by a power law fit of $dN_{ch}/d\eta|_{|\eta|<1} \propto N_{part}^{\alpha}$, with $\alpha = 1.07 \pm 0.04$.

3.3. Charged particle density in $|\eta| < 5.4$

Our data on $dN_{ch}/d\eta|_{|\eta|<1}$ clearly show a non-trivial evolution of the mid-rapidity particle density going from the most peripheral to the most central collisions. Further information on the underlying physics can be obtained by studying the change in particle production over a wider range in η. We performed this measurement using the PHOBOS multiplicity detector, consisting of the Octagon barrel covering $|\eta| \leq 3.2$ and the Ring counters detecting particles with $3 \leq |\eta| < 5.4$.

The number of charged particles traversing the detector was estimated based on the number and energy of hits in the silicon detectors, i.e. Si pixels showing a charge deposition above a certain threshold. Details of the hit-counting procedure and the background correction can be found in [13].

We performed this measurement for different centrality classes ranging from $\langle N_{part}\rangle = 83$ to $\langle N_{part}\rangle = 353$. For the most central 3% of the collisions we find an average number of charged particles of $4100 \pm 100(stat) \pm 400(syst)$ within $|\eta| < 5.4$.

Figure 4(a) shows the measured $dN_{ch}/d\eta$ distributions for three centrality bins, scaled by $0.5 \times N_{part}$. For comparison, the predictions of HIJING appear in Fig. 4(b). At mid rapidity, the non-central data are higher than the predictions, as shown earlier. Both data and HIJING show that the bulk of additional particle production in central collisions, as compared to peripheral ones, occurs near mid-rapidity. Whereas HIJING predicts that for large η the distributions should be roughly equal, the data show a clear sensitivity of $dN_{ch}/d\eta/(0.5 \times N_{part})$ on N_{part}, dropping by nearly a factor of two near $\eta = 5$. This demonstrates the presence of additional particle production mechanisms in the fragmentation region not described within HIJING. Also, the central plateau in the data is significantly wider than the HIJING prediction. Model comparisons with cascade models including rescattering of produced particles could help in resolving the source of

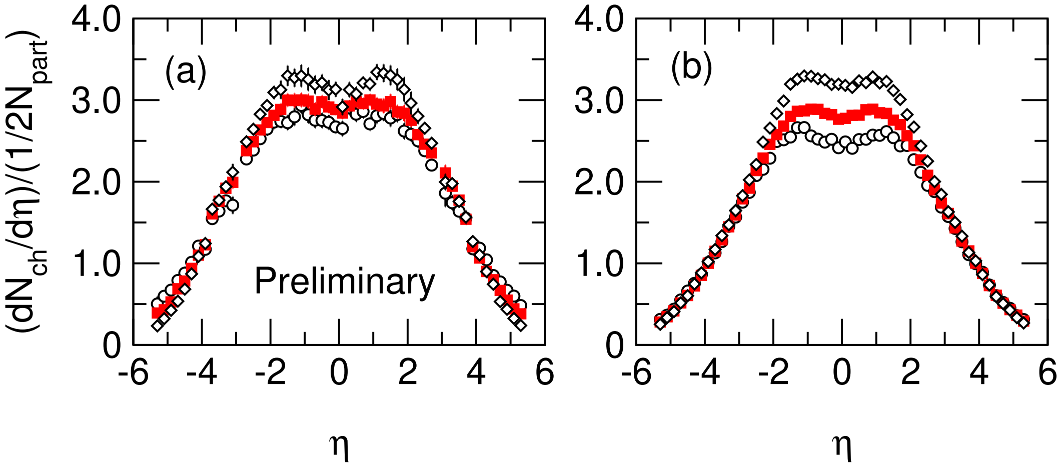

Figure 4. (a). Measured $dN_{ch}/d\eta/N_{pp}$ for N_{part}=102 (open circles), 216 (filled squares) and 354 (filled diamonds). (b). Same as (a) from HIJING. OFFICIAL STATEMENT ON SYST. ERROR GOES HERE.

this discrepancy.

4. Event Anisotropy

Based on hydrodynamical model calculations, it has been argued that a systematic study of the final state momentum anisotropy can provide a sensitive probe of the approach to local thermal equilibrium in the particle source in heavy ion collisions and also of the equation of state in the various stages of the collision [14,15].

The momentum space anisotropy, which is a reflection of the initial state space anisotropy for non-central collisions, is commonly quantified by the first and second Fourier coefficients of the azimuthal particle distribution relative to the reaction plane determined for every event, $dN/d(\phi - \Psi_R) = N_0(1 + \sum_i 2v_i \cos[n(\phi - \Psi_R)])$, where Ψ_R is the reaction plane angle. Usually, the first Fourier component (v_1) is referred to as directed flow and the second one (v_2) as elliptic flow. Both components have been observed and studied in detail at lower collision energies.

Early predictions of hadronic cascade models suggested that the elliptic flow should be of equal magnitude as that observed at collisions at the CERN SPS and therefore significantly below the limit expected for a system in local thermal equilibrium. For the directed flow a trivial decrease of the observed strength is expected based on the larger longitudinal momenta at the higher RHIC collision energies.

In PHOBOS, we have studied elliptic flow based on the azimuthal distribution of hits in the Octagon detector. For every event the event plane angle Ψ_R was determined by a fit to the azimuthal hit distribution. The observed raw value for v_2 was corrected for the effects of detector granularity, the resolution of the event-by-event determination of the event plane relative to the true reaction plane and the contribution of background hits. Details of the analysis can be found in [16].

We determined v_2 for events in seven classes of centrality, as determined using the paddle-mean described above. The resulting dependence on N_{part} is shown in Fig.5. We observed a strong centrality dependence of v_2 ranging from 0.03 for the most central events up to 0.07 for peripheral events. This follows the trend expected from the magnitude of the initial state spatial anisotropy. The values observed by PHOBOS are in good agreement with those reported by the STAR collaboration [17]. The maximum value of $v_2 = 0.07$ is about twice as big as v_2 obtained in Pb+Pb collisions at the SPS. Contrary to cascade code predictions, we observe a strong increase between SPS to RHIC energies, indicating a much closer approach to local thermal equilibrium. It is a matter of intense theoretical discussion at which stage in the collision process this equilibrium is established [15].

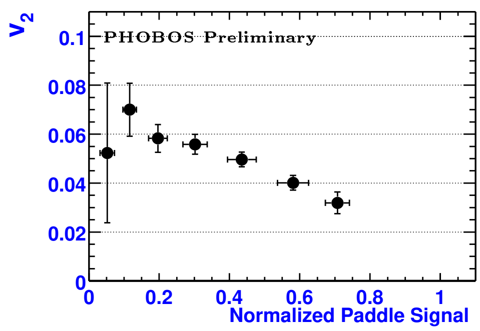

Figure 5. Elliptic flow, v_2, in the region -1.0< η <1.0 as a function of centrality. The error bars are statistical only. We estimate a systematic error of $\Delta v_2 = 0.007$.

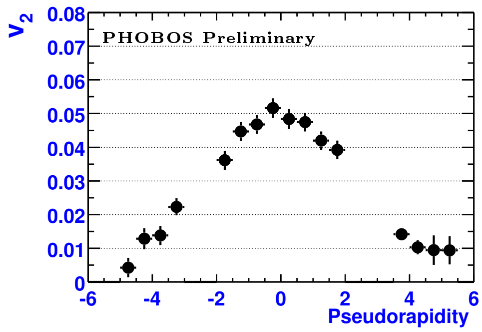

Figure 6. Elliptic flow, averaged over centrality, as a function of η. The error bars are statistical only. We estimate a systematic error of $\Delta v_2 = 0.007$.

4.1. Particle ratios

Using the mid-rapidity spectrometer, we have studied the ratios of multiplicities of particle and antiparticles for primary charged pions, kaons and protons at $\sqrt{s_{NN}} = 130$ GeV. In particular, the ratio of antibaryons to baryons plays a key role in understanding the properties of the hot and dense system formed in heavy-ion collisions at high energies. One of the most intriguing results from heavy-ion collisions at lower energies was the observation that particle ratios for particles with production cross-sections varying by several orders of magnitude could be described in an statistical equilibrium picture [18–20]. This is particularly remarkable in the case of rare baryons and antibaryons containing multiple strange quarks, which is difficult to describe in hadronic transport models using normal hadronic cross-sections. One of the key ingredients for the statistical particle production picture is the baryo-chemical potential μ_B, which can be extracted from our data.

On a microscopic level, the $\langle\overline{p}\rangle/\langle p\rangle$ ratio reflects the interplay between the transport of baryon number carried by protons and neutrons in the colliding nuclei in momentum space, the production of quark-antiquark pairs and the annihilation of antiprotons in the final stages of the collision.

The particle ratios were measured for an offline-selection of the 12% most central events, for which we estimate $\langle N_{part} \rangle = 312$. As the geometrical layout of the PHOBOS detector leads to an asymmetry in the acceptance and detection efficiency for positive and negatively charged particles in the same events, we used data taken with both polarities of the PHOBOS magnet. Thus most systematic effects like geometrical acceptance and tracking efficiency cancel when taking the ratio. This is particularly true if the number of positive and negative particles is approximately the same. This is ensured at RHIC, as the total number of charged particles is much bigger than the charge asymmetry in the initial state of the collision.

The raw particle ratios are corrected for particle decays and secondary interactions and the contribution from feed-down of strange hadrons. We find the following ratios within our acceptance:

$$
\begin{aligned}
\langle \pi^- \rangle / \langle \pi^+ \rangle &= 1.01 \pm 0.01(\text{stat.}) \pm 0.05(\text{syst.}) \\
\langle K^- \rangle / \langle K^+ \rangle &= 0.91 \pm 0.09(\text{stat.}) \pm 0.1(\text{syst.}) \\
\langle \overline{p} \rangle / \langle p \rangle &= 0.54 \pm 0.05(\text{stat.}) \pm 0.1(\text{syst.})
\end{aligned}
$$

Fig. 4.1 shows our results in comparison to data at lower energies [8,21,22] and calculations with the HIJING and RQMD [23] microscopic transport codes. We find significantly higher values for the $\langle K^- \rangle / \langle K^+ \rangle$ and $\langle \overline{p} \rangle / \langle p \rangle$ ratios than at lower energies. The HIJING

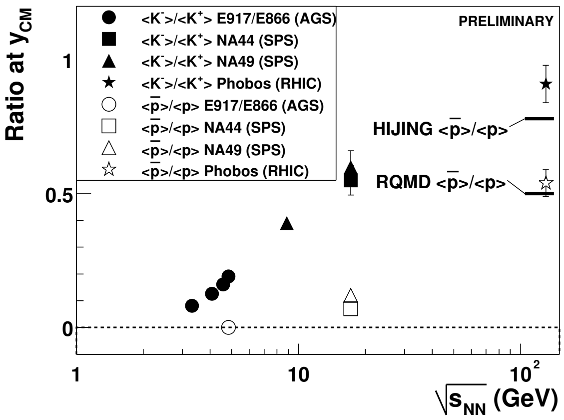

Figure 7. $\langle K^- \rangle / \langle K^+ \rangle$ and $\langle \overline{p} \rangle / \langle p \rangle$ ratios as a function of $\sqrt{s}$ for nucleus-nucleus collisions, in comparison with predictions from the HIJING and RQMD models. Only statistical errors are shown.

model overestimates the data by 30%. This comparison was made using the same parameters that successfully described the charged particle multiplicity density in central Au+Au collisions at RHIC [6], demonstrating that the particle ratio data provide additional constraints for microscopic models. A successful description may require a modification in either the baryon number stopping mechanism, baryon-pair production or antibaryon annihilation. An indication of possible mechanisms is given by the comparison with RQMD, which includes rescattering of produced hadrons and predicts a value for $\langle\overline{p}\rangle/\langle p\rangle$ that is 10% below our data point.

We estimated the baryo-chemical potential μ_B based on the $\langle K^-\rangle/\langle K^+\rangle$ and $\langle\overline{p}\rangle/\langle p\rangle$ ratios, using a statistical model calculation by Redlich et al. [24]. For a realistic range of freeze-out temperatures of 160 to 170 MeV, both ratios are consistent with $\mu_B = 50 \pm 10$ MeV. This is much lower than the value of $\mu_B = 270$ MeV obtained in thermal fits to Pb+Pb data from the CERN SPS [20], showing a closer but not yet complete approach to a baryon-free regime at RHIC.

5. Summary

We have presented data taken by the PHOBOS experiment at the first RHIC run. Our studies have shown that Au+Au collisions at RHIC produce the highest particle densities yet observed in heavy-ion collisions, exceeding the densities seen at the CERN SPS by 70%. Normalizing per participant pair, particle production at mid-rapidity is enhanced by 40% compared to $p\overline{p}$ collisions at the same energy. Model comparisons have shown that our data place very specific constraints on particle production mechanism. In particular the observed centrality dependence of $dN_{ch}/d\eta|_{|\eta|<1}/(0.5 \times N_{part})$, with a fast initial rise up to $\langle N_{part}\rangle = 80$, is different from the predictions of many popular models. Our study of the full pseudo-rapidity distribution up to $|\eta| = 5.4$ shows that much of the additional particle production is concentrated near mid-rapidity, consistent with the expectations of hard-scattering models. However, we also observe a somewhat wider plateau of the η distribution than predicted by e.g. HIJING and clear evidence for processes in the fragmentation region at large pseudo-rapidities that are not correctly modeled in this code.

One of the crucial questions in the understanding of interpretation of data from heavy-ion collisions is the validity of descriptions employing (local) equilibration. The data on elliptic flow show, that the interactions in the produced collision system very effectively transform the initial state spatial anisotropy into a final state momentum space anisotropy. Comparisons with hadronic cascade models suggest that this interaction must happen in the early, dense state of the system to achieve the observed values of elliptic flow.

Finally, we have taken a first step towards characterizing the hadro-chemical composition of the particle source by measuring antiparticle/particle ratios at mid-rapidity. These ratios can be related to the baryo-chemical potential μ_B in statistical models of particle production. Our ratios indicate a value of $\mu_B = 50$ MeV, about a factor of 5 smaller than observed at SPS energies. The particle source at RHIC therefore has a significantly smaller net baryon-density than at lower energies, but still is not in a regime that could be described as completely baryon-free.

Based on these initial results characterizing the global conditions achieved in heavy-ion collisions at RHIC, we hope to see detailed theoretical predictions for the 2001 running period at RHIC, where we expect to collect 100 times larger statistics than in the initial running. This will allow a detailed investigation of two-particle correlations and particle distributions at low and high transverse momenta and the search for non-statistical event-by-event distributions. We expect that a scan of the observables shown here as a function of collision energy and nuclear species will also be an important part of the near-term

RHIC program.

Acknowledgements: This work was partially supported by: (US) DoE grants DE-AC02-98CH10886, DE-FG02-93ER40802, DE-FC02-94ER40818, DE-FG02-94ER40865, DE-FG02-99ER41099 and W-31-109-ENG-38, NSF grants 9603486, 9722606 and 0072204, (Poland) KBN grant 2 P03B 04916, (Taiwan) NSC contract NSC 89-2112-M-008-024.

REFERENCES

1. See for example J.P.Blaizot, Nucl. Phys. **A661** (1999) 3.
2. B.Back et al., Nucl. Phys. **A661** (1999) 690.
3. R. Pak et al., see proceedings of this conference.
4. M.Gyulassy and X.N.Wang, Comp. Phys. Comm. 83 (1994) 307. We used HIJING V1.35 with standard parameter settings.
5. J. Katzy et al., PHOBOS coll. see proceedings of this conference.
6. B. B. Back, et al., Phys. Rev. Lett. **85** 3100 (2000).
7. F.Abe et al., Phys. Rev. **D41** (1990) 2330.
8. J. Bächler et al., Nucl. Phys. **A661** (1999) 45.
9. J.D.Bjorken, Phys. Rev. **D27** (1983) 140.
10. X. Wang and M. Gyulassy, nucl-th/0008014.
11. K. J. Eskola, K. Kajantie, P. V. Ruuskanen and K. Tuominen, Nucl. Phys. **B570**, 379 (2000) [hep-ph/9909456].
12. M. M. Aggarwal et al., WA98 coll., nucl-ex/0008004.
13. A. Wuosmaa et al., PHOBOS coll. see proceedings of this conference.
14. J.-Y. Ollitrault, Phys. Rev. **D46** 229 (1992).
15. D. Teaney, J. Lauret, E.V. Shuryak, nucl-th/0011058
16. I. C. Park et al., PHOBOS coll. see proceedings of this conference.
17. K. Ackermann, STAR coll. Phys. Rev. Lett. 86 (2001) 402.
18. E. Schnedermann, J. Sollfrank, U. Heinz, Phys. Rev. bf C48 (1993) 2462.
19. F. Becattini, Z. Phys. **C69** (1996) 485.
20. P. Braun-Munzinger, I. Heppe, J. Stachel, Phys. Lett. **B465** (1999) 15.
21. L. Ahle et al., E866 and E917 Collaborations, PLB 490 (2000) 53.
22. I. G. Bearden et al. Phys. Lett. **B388** (1996) 431.
23. H. Sorge, Phys. Rev. **C52** (1995) 3291.
24. K. Redlich, see proceedings of this conference